APPLIED SCIENCES AND ENGINEERING

10.1126/sciadv.1600978

Controlled deformation of vesicles by flexible structured media

Rui Zhang,[1] Ye Zhou,[1] José A. Martínez-González,[1] Juan P. Hernández-Ortiz,[2] Nicholas L. Abbott,[3] Juan J. de Pablo[1]*

Liquid crystalline (LC) materials, such as actin or tubulin networks, are known to be capable of deforming the shape of cells. Here, elements of that behavior are reproduced in a synthetic system, namely, a giant vesicle suspended in a LC, which we view as a first step toward the preparation of active, anisotropic hybrid systems that mimic some of the functionality encountered in biological systems. To that end, we rely on a coupled particle-continuum representation of deformable networks in a nematic LC represented at the level of a Landau–de Gennes free energy functional. Our results indicate that, depending on its elastic properties, the LC is indeed able to deform the vesicle until it reaches an equilibrium, anisotropic shape. The magnitude of the deformation is determined by a balance of elastic and surface forces. For perpendicular anchoring at the vesicle, a Saturn ring defect forms along the equatorial plane, and the vesicle adopts a pancake-like, oblate shape. For degenerate planar anchoring at the vesicle, two boojum defects are formed at the poles of the vesicle, which adopts an elongated, spheroidal shape. During the deformation, the volume of the topological defects in the LC shrinks considerably as the curvature of the vesicle increases. These predictions are confirmed by our experimental observations of spindle-like shapes in experiments with giant unilamellar vesicles with planar anchoring. We find that the tension of the vesicle suppresses vesicle deformation, whereas anchoring strength and large elastic constants promote shape anisotropy.

INTRODUCTION

The physics of colloidal suspensions in liquid crystals (LCs) has attracted considerable interest (*1*, *2*). When dispersed in a nematic LC, rigid spherical particles can induce certain disclinations (*3*, *4*) and self-organize into intriguing patterns (*2*, *5*–*13*). Similarly, recent work with nonspherical particles in nematic LCs has revealed a wide range of previously unknown self-assembled structures (*14*–*17*). In the context of cell biology, it is well known that tubulin or actin polymerization can deform the shape of cells, vesicles, or even liquid droplets, leading to the formation of highly anisotropic shapes (*18*, *19*). Previous theoretical studies suggest that, in the weak anchoring limit, isotropic droplets immersed in a LC can be deformed by the medium, provided that the interfacial tension is sufficiently low (as in the presence of surfactants) (*20*–*22*). Similarly, within a smectic LC, experiments and numerical calculations indicate that soft deformable particles may adopt an elongated shape (*23*, *24*). The inverse problem, namely, that of the shape adopted by a nematic LC droplet within an isotropic solution (a "tactoid"), has also been investigated for a variety of conditions (*25*–*28*). More recent studies have considered deformation of lyotropic chromonic LC (LCLC) droplets and even active nematics (*29*, *30*).

In contrast, the case of a LC droplet or a LC-filled vesicle in a nematic LC has not been addressed before. However, this system is of particular interest because it provides a promising platform for the development of active, responsive materials. In a LC droplet, the surface tension depends on the local director. Its shape can be obtained from a Wulff construction (*31*). For isotropic deformable particles in a nematic LC, the particle shape interacts with the defect structure through the underlying director field; determining the equilibrium shape in the presence of such coupling interactions remains an unsolved problem, which we address in this work.

A lipid vesicle generally consists of a lipid bilayer membrane that encapsulates an aqueous solution (*32*). Vesicle shape can deform, but the dynamics are different from that of a liquid droplet. A theoretical model of soft solids interacting within a nematic LC was originally proposed by Rey (*33*), and, to the best of our knowledge, only one published study has presented simulations of vesicle deformation in a nematic LC (*34*). The latter work focused on rigid (infinite) homeotropic anchoring in two dimensions, thereby precluding direct comparison or application to easily accessible experimental systems.

Here, we examine how surface properties and LC elastic constants affect vesicle deformation, and we pay special attention to the resultant disclination structures that arise from surface deformation. To do so, we rely on full three-dimensional simulations of a nematic LC that is treated at the level of a Landau–de Gennes free energy functional for the order parameter tensor **Q**. The vesicle is described as a bead-spring network "shell" whose equilibrium shape is altered as the bulk and surface forces arising from elasticity and anchoring seek to balance each other. We propose an equation to calculate surface forces due to surface torques arising from finite anchoring, and we find that different surface stress calculations reported in the literature are essentially equivalent (*34*, *35*). Our findings suggest new avenues for control of colloidal self-assembly structure by tuning the underlying particle shape through, for instance, temperature changes (*15*). The predictions of our calculations are validated by experimental measurements which indicate that, when immersed in LCLCs, giant vesicles can be deformed as anticipated in our simulations.

[1]Institute for Molecular Engineering, University of Chicago, Chicago, IL 60637, USA. [2]Departamento de Materiales, Universidad Nacional de Colombia, Medellin 050034, Colombia. [3]Department of Chemical and Biological Engineering, University of Wisconsin-Madison, Madison, WI 53706, USA.
*Corresponding author. Email: depablo@uchicago.edu

RESULTS

The vesicle, which is represented by a bead-spring network having 2562 beads and 7680 springs, is initialized as a sphere of radius $R = 16$. It is placed at the center of a LC channel of size $[X, Y, Z] = [100, 100, 100]$, which is bounded by a top and a bottom wall whose normals are in the z-direction. To fix the far-field LC director $\mathbf{n}_0$, non-degenerate planar anchoring along the y-direction is enforced at both walls. The characteristics of the model are chosen such that an undistorted LC scalar order parameter $q_0 \approx 0.6$ is obtained, a value that is consistent with that encountered in typical experimental observations (see Materials and Methods). We refer by "homeotropic vesicle" and "planar vesicle" to vesicles that exhibit homeotropic (normal) and degenerate planar (tangential) anchoring conditions, respectively. The system is assumed to reach equilibrium when the free energy is minimized by a Ginzburg-Landau approach.

We first examine the local stress on the surface before the vesicle deforms. Results for planar and homeotropic anchoring conditions for either strong or weak anchoring strength (W) are shown in Fig. 1. For strong anchoring, the force is more pronounced near the defect. The force points outward from the vesicle, thereby causing the vesicle surface to be pulled toward the defect. For weak anchoring, the force magnitude is small and evenly distributed throughout the surface. For planar anchoring, the regions near the two boojums experience a pulling force, but the equator experiences a pushing force. In contrast, for a Saturn ring defect, the equator experiences a pulling force, and the poles experience a pushing force. The physical origins of these forces are discussed in what follows.

The defect structures associated with the vesicle at different times are shown in Fig. 2. After the LC-induced deformation, two correlated processes take place. First, the defect volume, which is characterized by the volume of a low-scalar order parameter region (with scalar order parameter $q < 0.3$), shrinks and eventually becomes too small to resolve with our finite-difference mesh. For homeotropic anchoring, the

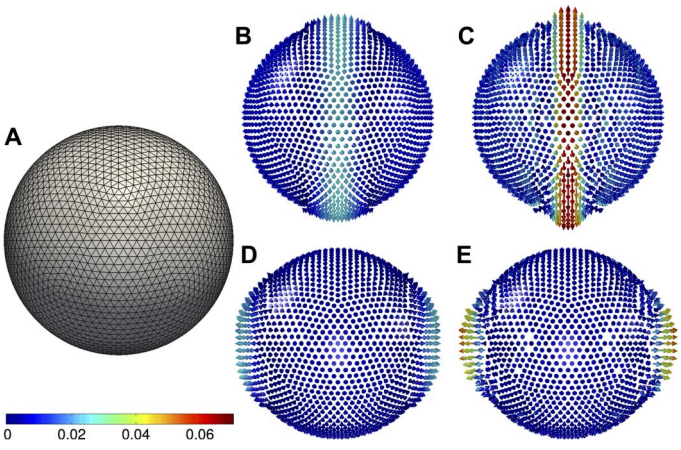

Fig. 1. The vesicle network and the underlying force distribution exerted by the nematic LC before deformation. (**A** to **E**) Vesicle network (A) and stress distribution on vesicle before deformation for ring (B and C) and boojum (D and E) defects. Anchoring strength: 3×10^{-4} N/m (B and D) and 3×10^{-3} N/m (C and E). The stress unit is 1.27×10^{-7} N/μm^2.

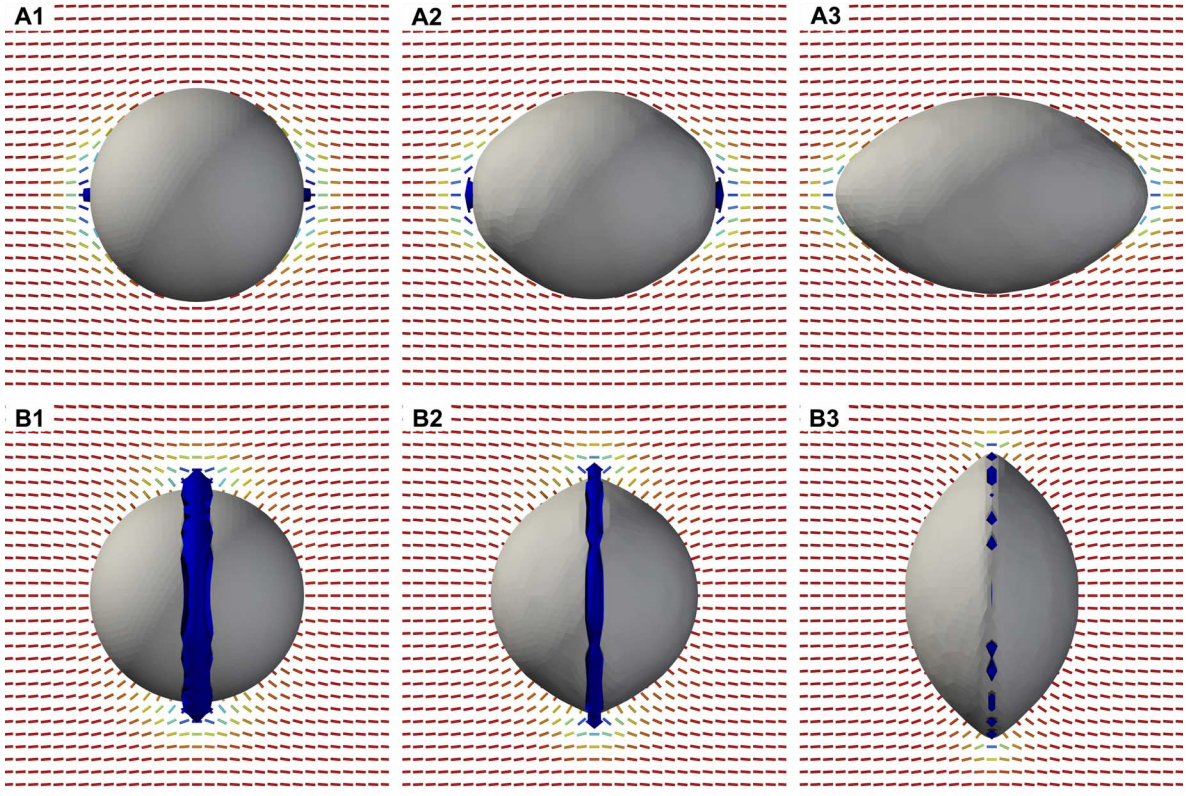

Fig. 2. Defect structure for a deformed vesicle with $k_{str} = 2.0$, $k_{curv} = 2.0$, and $k_{vol} = 10.0$ and anchoring strength $W = 10^{-3}$ N/m. (**A**) Homeotropic vesicle shape evolution from (A1) through (A2), and equilibrium shape in (A3). (**B**) Degenerate planar vesicle shape evolution from (B1) to (B2) and equilibrium as (B3).

ring defect becomes disconnected, and for planar anchoring, the boojum defect volume shrinks. Second, the local curvature in the region near the defect increases: the homeotropic vesicle expands and adopts a pancake shape at the equator, where the ring defect is localized, and the planar vesicle becomes elongated along the two boojum (point) defects. These two processes are correlated because the surface curvature suppresses the topological defect(s), and the defect(s) raises the total free energy. Consider, for example, a radius of curvature r. If $r \geq \xi_{Kd} = K/W$ (see Materials and Methods for a discussion on Kleman–de Gennes length ξ_{Kd}), surface anchoring is able to distort the director field and produce a topological defect; if $r < \xi_{Kd}$, LC elasticity overcomes surface anchoring and the defect is less well defined, having a higher scalar order parameter. In some cases, it is smaller than the grid size. As shown in Fig. 3, the system's elastic and surface energy decreases during deformation. We hypothesize that the vesicle attempts to release elastic energy by increasing the local curvature of the region near the high elastic distortion space, namely, the defect. The resultant shape is further defined by this trend, along with the constraints of fixed vesicle volume and surface area.

We also performed simulations of vesicle deformation with LC on both sides of the surface. Representative snapshots are shown in Fig. 4. For homeotropic anchoring, before deformation, there is a point defect located at the center of the vesicle. After deformation, the inner defect transforms into a ring defect at the inlet of the network because of curvature effects. The outer ring defect expands and becomes disconnected. Similarly, for the planar anchoring case, as the vesicle elongates along the director field, the two boojum defects are displaced toward the vesicle interior. Despite the difference in defect structure, the shape of the different types of vesicles is consistent with that of vesicles with an unstructured (non-LC) fluid in the interior. Our predictions of planar anchoring vesicle shape are confirmed by experiments with a giant unilamellar vesicle (GUV) immersed in LCLCs. The GUVs were prepared from a ternary mixture (1 mM total lipid concentration) of 1,2-dioleoyl-*sn*-glycero-3-phosphocholine (DOPC; at 97.5 mol %), 1,2-dioleoyl-*sn*-glycero-3-phosphoethanolamine-*N*-[methoxy(polyethylene glycol)-2000] (ammonium salt) (DOPE-PEG2000; at 2 mol %), and *N*-(4,4-difluoro-5,7-dimethyl-4-bora-3a,4a-diaza-*s*-indacene-3-propionyl)-1,2-dihexadecanoyl-*sn*-glycero-3-phosphoethanolamine triethylammonium salt (BODIPY-DHPE; at 0.5 mol %) in either 5.5 weight % (wt %) or 15% of disodium cromoglycate (DSCG). As can be observed in Fig. 5, in isotropic solutions containing 5.5 wt % DSCG, the GUVs adopt spherical shapes (Fig. 5A). In the nematic phases, which appear for 15 wt % DSCG, we observe that the GUVs become elongated and spindle-shaped (Fig. 5B), as predicted by the simulations. These observations serve to confirm that the elasticity of the LC does indeed compress the GUV along the GUV axis perpendicular to the local director.

We next consider the effect of surface elasticity k_{str} and bending modulus k_{curv} on vesicle shape. A value of $k_{vol} = 10.0$ is adopted to ensure volume conservation. For all the conditions considered here, the total volume change is less than 0.1%. To quantify vesicle shape, we measure the aspect ratio $a_S = D_y/D_z$, where D_y and D_z are the projected lengths of the vesicle along the y- and z-directions. We also calculate the anisotropy of the moment of inertia, which is defined as $a_m = I_y/I_z$, where I_y and I_z are the moment of inertia with respect to the y and z axis, respectively. For the results shown in Fig. 6A, we keep $k_{str} = k_{curv} = k$. For weaker k, the vesicle undergoes a more pronounced deformation, a_m reaches a plateau when $k \leq 1$, and a_S appears to be linear with respect to $\log(k)$ even at low k. To ensure that the vesicle surface is inextensible, we choose $k_{str} = 32.0$ and vary k_{curv} in Fig. 6B. Again, the bending coefficient k_{curv} prevents deformation (it penalizes surface curvature). The largest anisotropy that one can generate with a high k_{str} is 1.1 (or 0.9 for a pancake shape), compared to as high as 1.4 (or 0.7 for the opposite situation) for the $k_{str} = k_{curv}$ case.

Figure 6C shows the results for the effect of surface anchoring. For weak and moderate anchoring ($W < 10^{-3}$ N/m), W promotes surface deformation. For strong anchoring conditions, shape anisotropy reaches a plateau value of 1.25 (or 0.8 for homeotropic vesicles). For strong anchoring, the corresponding Kleman–de

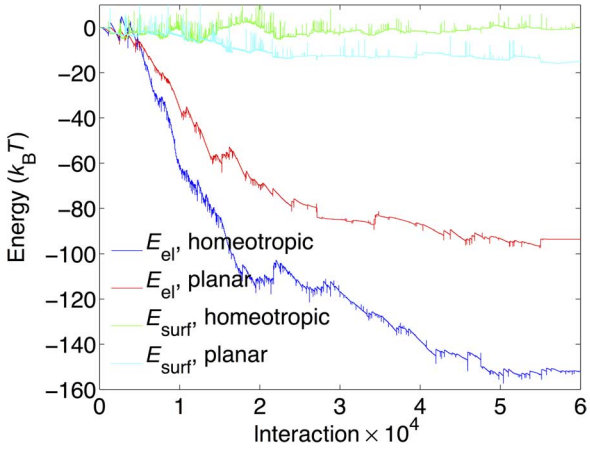

Fig. 3. Temporal behavior of the elastic energy and surface energy during vesicle deformation for anchoring $W = 10^{-3}$ N/m and constants $k_{str} = 2.0$, $k_{curv} = 2.0$, and $k_{vol} = 10.0$.

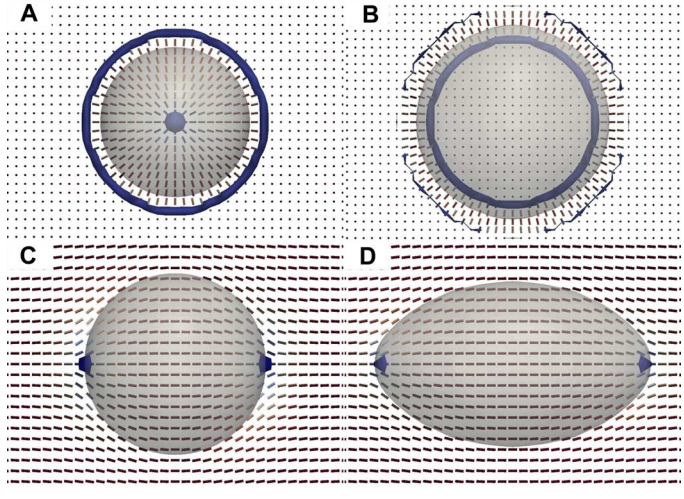

Fig. 4. Morphology of vesicle with homeotropic and degenerate planar anchoring before and after deformation when LC is found both inside and outside the membrane. (**A** and **B**) Shape of the homeotropic vesicle, with the corresponding defect structure. (**C** and **D**) Shape of the planar vesicle with its defect structure.

Genns length ξ_{Kd} drops below the nematic coherent length ξ, and the LC phase becomes less sensitive to anchoring. Hence, the surface force saturates.

Vesicle deformation originates from the anisotropic elastic stress generated by the LC. As the elastic constant weakens, this force should be weaker. This correspondence is shown in Fig. 6D. To eliminate the effect of varying the LC phase by changing the elastic constant L_1, here, we only consider the strong anchoring case as if the vesicle surface exhibits rigid anchoring. The vesicle shape anisotropy becomes negligible when L_1 drops two orders of magnitude.

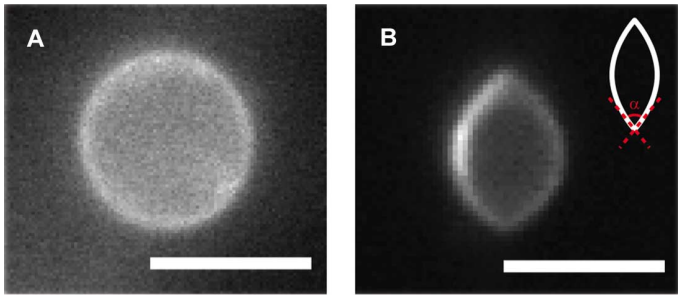

Fig. 5. Experimental observations of the straining of vesicles in a nematic medium. (**A** and **B**) Fluorescence images of GUV within an (A) isotropic solution of 5.5 wt % DSCG and a (B) nematic solution of 15 wt % DSCG at room temperature. In an isotropic environment, GUVs adopt a spherical shape, whereas in a nematic environment, the elastic forces distort the GUV into a spindle shape, with a cusp angle of $\alpha \approx 107°$. We note that (A) and (B) are not the same GUV. Scale bars, 5 μm.

CONCLUSIONS

Here, theories and simulations have been used to determine the shape adopted by flexible vesicles suspended in nematic LCs. We have examined the effects of various anchoring conditions and that of the LC elastic coefficients. Regardless of whether the interior of the vesicles is structured or unstructured, planar vesicles favor elongated (prolate) shapes. The elongation follows the far-field LC director. Our predictions for planar anchoring are confirmed by measurements of GUVs in a LCLC. In contrast, homeotropic vesicles with quadrupolar structure favor a pancake (oblate) shape, with the minor axis oriented along the far-field LC director. We hypothesize that the surface torque that originates from elastic distortions provides the driving force for the deformation. The vesicle shape is quantified by the ratio of moments of inertia along different axes. We find that the shape anisotropy is suppressed by the vesicle surface elastic and bending moduli but is promoted by the surface anchoring strength and LC elastic constants.

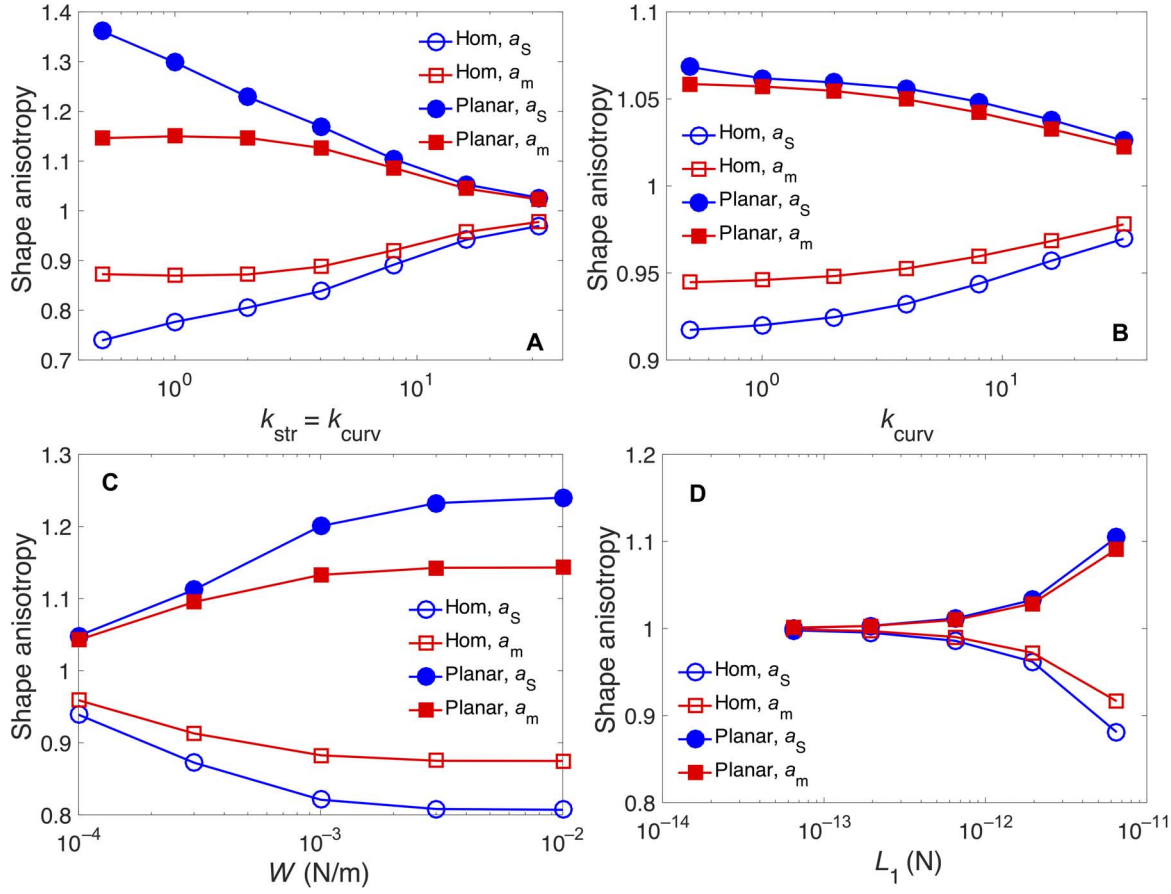

Fig. 6. Shape anisotropy with fixed $k_{vol} = 10.0$. (**A**) $k_{str} = k_{curv}$ is varied with $W = 10^{-3}$ N/m. (**B**) k_{curv} is varied with fixed $k_{str} = 32.0$ and $W = 10^{-3}$ N/m. (**C**) W is varied with $k_{str} = k_{curv} = 2.0$. (**D**) LC elasticity L_1 is varied with $k_{str} = k_{curv} = 2.0$ and $W = 3 \times 10^{-3}$ N/m.

MATERIALS AND METHODS

The vesicle model adopted in this work consists of a bead-spring shell (*34*, *36*–*38*). All simulations begin with a spherical vesicle of radius R, which is built by a triangular network. The vertices of the network are the beads, and the springs that connect neighboring sites control surface elasticity. The mass of each node is denoted by m, and there are N nodes in the network. The energy of the vesicle includes three contributions, namely

$$E^{\text{vesicle}} = E^{\text{elastic}} + E^{\text{volume}} + E^{\text{bending}}$$

Surface stretch (surface area expansion) is penalized by the elastic energy, which only applies to neighboring beads P_i and P_j that are connected by a spring. E^{elastic} takes the following form

$$E^{\text{elastic}} = \sum_{\text{neighbor } (i,j)} E_{ij}^{\text{elastic}} = \sum_{\text{neighbor } (i,j)} \frac{1}{2} k_{\text{str}} (r_{ij} - r_{ij}^0)^2$$

where r_{ij} and $r^0{}_{ij}$ are the instantaneous and the equilibrium spring lengths connecting bead (node) P_i and P_j, respectively. The corresponding elastic coefficient for stretching is denoted by k_{str}.

Given the surface normal ν, the vesicle volume V can be expressed as a surface integral

$$V = \frac{1}{3} \int_S \mathbf{r} \cdot \boldsymbol{\nu} dS$$

To numerically calculate V, the following expressions are used

$$V \cong \frac{S}{3N} \sum_{i=1}^{N} \mathbf{r}_i \cdot \boldsymbol{\nu}_i = \frac{1}{6N} \sum_{(i,j)} \mathbf{r}_{ij} b_{ij} \sum_{i=1}^{N} \mathbf{r}_i \cdot \boldsymbol{\nu}_i \quad (1)$$

where $\mathbf{r}_i$ and $\boldsymbol{\nu}_i$ are the position vector and the surface normal at node P_i, respectively. Specifically, $\boldsymbol{\nu}_i$ is the normal to the best-fit surface s_i crossing all the neighbor beads around P_i. Additional details about how to determine s_i are provided in section A of the Supplementary Materials. The variable b_{ij} represents the reciprocal length of edge $\mathbf{r}_{ij}$. If $\mathbf{r}_{ij}$ is the side of two triangles $P_iP_jP_l$ and $P_iP_jP_k$, the centers of the corresponding circumscribed circles are denoted by Q_{ijk} and Q_{ijl}. The middle point of P_iP_j is, namely, R_{ij}. Vectors $Q_{ijk}R_{ij}$ and $Q_{ijl}R_{ij}$ are perpendicular to P_iP_j. The reciprocal length of P_iP_j is defined as $b_{ij} = |Q_{ijk}R_{ij}| + |Q_{ijl}R_{ij}|$. A graphical illustration of b_{ij} is provided in section C of the Supplementary Materials.

The energy penalty associated with a volume change is given by

$$E^{\text{volume}} = \frac{1}{2} k_{\text{vol}} (V - V_0)^2$$

where V_0 is the initial volume (original volume before immersed in LC), and k_{vol} is related to the compressibility $\beta = -\frac{1}{V}\frac{\partial V}{\partial P} = 1/Vk_{\text{vol}}$, where P is the pressure. A large value of k_{vol}, which is akin to the compressibility, serves to enforce a constant volume.

The bending energy due to surface curvature is written as

$$E^{\text{bending}} = \frac{1}{2} k_{\text{curv}} \sum_i d_i^2$$

where d_i is the distance from node P_i to its associated surface s_i, and k_{curv} is the coefficient that penalizes bending of the membrane. If the vesicle surface is flat, $d_i = 0$, and the bending energy vanishes. The bending energy is nonzero for curved interfaces and leads to a contribution to the surface tension by $\gamma_{\text{bend}} = k_{\text{curv}}/\sqrt{3}$. The k_{str} and k_{curv} spring constants have units of energy/length^2, and k_{vol} has units of energy/length^6.

The structure of the LC is described in terms of a $\mathbf{Q}$-tensor (*39*). The total free energy F of the LC is given by

$$F = \int_{\text{bulk}} dV (f_{\text{Ld}} + f_{\text{E}}) + \int_{\text{surface}} dS f_{\text{S}}$$

By introducing an energy scale A_0 and a parameter U, one can write the Landau–de Gennes free energy density f_{Ld} as (*35*)

$$f_{\text{Ld}} = \frac{A_0}{2}\left(1 - \frac{U}{3}\right)\text{Tr}(\mathbf{Q}^2) - \frac{A_0 U}{3}\text{Tr}(\mathbf{Q}^3) + \frac{A_0 U}{4}[\text{Tr}(\mathbf{Q}^2)]^2$$

Here, A_0 corresponds to the core energy of a LC defect, and U is related to concentration for lyotropic LCs and temperature for thermotropic LCs. A value of $U = 3.5$ is adopted in this work. The scalar order parameter q_0 of an undistorted nematic LC is related to U by

$$q_0 = \frac{1}{4} + \frac{3}{4}\sqrt{1 - \frac{8}{3U}}$$

The elastic (distortion) energy density of the LC is denoted by f_{E}. Within the single elastic constant approximation L_1, f_{E} is (*35*) given by

$$f_{\text{E}} = \frac{1}{2} L_1 (\nabla \mathbf{Q})^2$$

where L_1 is related to the Frank elastic constant K by $K = 2q_0{}^2 L_1$.

The surface anchoring energy is denoted by f_{S}. For a surface anchoring strength W and nondegenerate anchoring, it is given by the Rapini-Papoular form (*40*)

$$f_{\text{S}} = \frac{1}{2} W (\mathbf{Q} - \mathbf{Q}^{\text{S}})^2$$

where $\mathbf{Q}^{\text{S}}$ is the preferred $\mathbf{Q}$-tensor at the surface. For degenerate planar anchoring, f_{S} is given by the Fournier-Galatola form (*41*)

$$f_S = W(\tilde{\mathbf{Q}} - \tilde{\mathbf{Q}}^{\perp})^2$$

where $\tilde{\mathbf{Q}} = \mathbf{Q} + (q_0/3)\mathbf{I}$ and $\tilde{\mathbf{Q}}^{\perp} = \mathbf{P}\tilde{\mathbf{Q}}\mathbf{P}$. $\mathbf{I}$ is the identity tensor. $\mathbf{P}$ is the projection operator associated with the surface normal ν as $\mathbf{P} = \mathbf{I} - \boldsymbol{\nu}\boldsymbol{\nu}$. The $\mathbf{Q}$-tensor of the LC is evolving according to the Euler-Lagrange equation on a cubic mesh by a finite-difference method (*39*). The equilibrium conditions are given by

$$\frac{\partial F}{\partial \mathbf{Q}} - \nabla \frac{\partial F}{\partial \nabla \mathbf{Q}} = 0 \quad \text{(bulk)}$$

and

$$\frac{\partial F}{\partial \nabla \mathbf{Q}} \cdot \boldsymbol{\nu} = 0 \qquad \text{(surface)}$$

Each bead P_i, having a point mass m, obeys the following equation of motion

$$m\ddot{\mathbf{r}} = -\frac{\partial E^{\text{vesicle}}}{\partial \mathbf{r}_i} + \mathbf{F}_i^{\text{ext}} - \gamma \mathbf{v}_i \qquad (2)$$

where $\mathbf{F}_i^{\text{ext}}$ is the external force exerted by the LC on bead P_i, γ is a friction coefficient, and $\mathbf{v}_i$ is the bead velocity. For an overdamped system, $\gamma \mathbf{v}_i = -\frac{\partial E^{\text{vesicle}}}{\partial \mathbf{r}_i} + \mathbf{F}_i^{\text{ext}}$. If there is no external force acting on the vesicle, surface tension acts to maintain a spherical shape. However, the LC surrounding the vesicle exerts an anisotropic stress that can induce a deformation. The antisymmetric portion of the surface stress gives rise to a surface torque. This torque (per area) $\boldsymbol{\Gamma}$ can be expressed as (*34*)

$$\Gamma_\alpha = \varepsilon_{\alpha\beta\gamma}\tau_{\beta\gamma} \qquad (3)$$

where $\varepsilon_{\alpha\beta\gamma}$ is the three-dimensional Levi-Civita symbol, and the Einstein summation convention is assumed. By introducing the surface molecular field $\mathbf{H}^W = W(\mathbf{Q} - \mathbf{Q}^S)$, a stress $\boldsymbol{\tau}$ is defined as

$$\boldsymbol{\tau} = \mathbf{Q}\mathbf{H}^W - \mathbf{H}^W\mathbf{Q}$$

We show in section B of the Supplementary Materials that multiple disparate expressions (*34*, *35*) for the anchoring-induced surface torque can, in fact, be reduced into a single expression. The spatial variation of the torque leads to a local stress, which is responsible for a surface deformation. In particular, the local stress is

$$\mathbf{F}^{\text{torq}} = \boldsymbol{\nu} \cdot \nabla \times \boldsymbol{\Gamma}$$

In section C of the Supplementary Materials, we explain in detail how to numerically calculate the stress distribution.

The symmetric portion of the surface stress, that is, the surface pressure, also contributes to the deformation of the surface. Such pressure (per area) p_S is (see the Supplementary Materials for details) given by

$$p_S = f - \boldsymbol{\nu} \cdot \nabla f_S(\mathbf{Q}) \qquad (4)$$

where $f = f_{\text{Ld}} + f_E$, and $f_S(\mathbf{Q})$ is a function of $\mathbf{Q}$ given by

$$f_S(\mathbf{Q}) = \frac{W}{2}(\mathbf{Q} - \mathbf{Q}^S)^2$$

The bead-spring network and the LC are coupled, as described in what follows. (i) The bead-spring network determines the topology of the LC mesh: any LC point that is in the vicinity of the network is regarded as surface-LC points. The points outside the network are the bulk-LC point. The interior points of the network can be either non-LC or bulk-LC points, depending on the choice of the material inside the vesicle. (ii) LC forces are applied to vesicle nodes through springs: the eight corners of a unit cubic cell in which the spring's middle point resides are the neighbors of the spring (or equivalently the neighbors of the two end nodes of the spring). The surface torque and force are first added to the spring with a weight proportional to the opposite volume from the point to the overall cell (*42*). The force is then equally distributed to the two end nodes, and two opposite forces are added to them; thus, the resultant torque is equal to the applied torque (*34*). (iii) The surface normal of the LC surface point is given by its neighboring vesicle nodes. If a given node happens to have no neighboring node, its nearest node's normal is assigned. The coupled system is evolved until the beads come to rest.

It is important to briefly mention two characteristic length scales. The Kleman–de Gennes length is defined as $\xi_{\text{Kd}} = K/W$ (*35*). If $\xi_{\text{Kd}} \gg R$, the distortion to the director field by the presence of a particle is negligible; otherwise, the distortion leads to formation of a point or line defect. The other length scale, $a = K/\gamma_S$, describes the competition between surface tension ($\sim\gamma_S R$) and elastic distortion ($\sim K$) (*43*). If $R \gg a$, the surface remains spherical; otherwise, elastic forces induce a deformation. Here, we focused on relatively strong anchoring and low surface tension, which are the conditions that are most easily realized in phospholipid vesicles suspended in chromonic LCs. Thus, $R \geq \xi_{\text{Kd}}$ and $R = \mathrm{O}(a)$.

SUPPLEMENTARY MATERIALS

Supplementary material for this article is available at http://advances.sciencemag.org/cgi/content/full/2/8/e1600978/DC1

A. Calculation of the best-fit surface in bead-spring model

B. Analytical expressions for LC surface torque and pressure

C. Surface torque to force calculation

fig. S1. Illustration of the stress calculation due to surface torque.

Reference (*44*)

REFERENCES AND NOTES

1. H. Stark, Physics of colloidal dispersions in nematic liquid crystals. *Phys. Rep.* **351**, 387–474 (2001).
2. I. Muševič, M. Škarabot, U. Tkalec, M. Ravnik, S. Žumer, Two dimensional nematic colloidal crystals self-assembled by topological defects. *Science* **313**, 954–958 (2006).
3. O. Guzmán, E. B. Kim, S. Grollau, N. L. Abbott, J. J. de Pablo, Defect structure around two colloids in a liquid crystal. *Phys. Rev. Lett.* **91**, 235507 (2003).
4. I. I. Smalyukh, O. D. Lavrentovich, A. N. Kuzmin, A. V. Kachynski, P. N. Prasad, Elasticity-mediated self-organization and colloidal interactions of solid spheres with tangential anchoring in a nematic liquid crystal. *Phys. Rev. Lett.* **95**, 157801 (2005).
5. P. Poulin, H. Stark, T. C. Lubensky, D. A. Weitz, Novel colloidal interactions in anisotropic fluids. *Science* **275**, 1770–1773 (1997).
6. J.-C. Loudet, P. Barois, P. Poulin, Colloidal ordering from phase separation in a liquid-crystalline continuous phase. *Nature* **407**, 611–613 (2000).
7. F. R. Hung, O. Guzmán, B. T. Gettelfinger, N. L. Abbott, J. J. de Pablo, Anisotropic nanoparticles immersed in a nematic liquid crystal: Defect structures and potentials of mean force. *Phys. Rev. E* **74**, 011711 (2006).
8. F. R. Hung, B. T. Gettelfinger, G. M. Koenig Jr., N. L. Abbott, J. J. de Pablo, Nanoparticles in nematic liquid crystals: Interactions with nanochannels. *J. Chem. Phys.* **127**, 124702 (2007).
9. T. Araki, H. Tanaka, Colloidal aggregation in a nematic liquid crystal: Topological arrest of particles by a single-stroke disclination line. *Phys. Rev. Lett.* **97**, 127801 (2006).
10. A. Nych, U. Ognysta, M. Škarabot, M. Ravnik, S. Žumer, I. Muševič, Assembly and control of 3D nematic dipolar colloidal crystals. *Nat. Commun.* **4**, 1489 (2012).
11. M. Ravnik, M. Škarabot, S. Žumer, U. Tkalec, I. Poberaj, D. Babič, N. Osterman, I. Muševič, Entangled nematic colloidal dimers and wires. *Phys. Rev. Lett.* **99**, 247801 (2007).
12. M. Rahimi, T. F. Roberts, J. C. Armas-Pérez, X. Wang, E. Bukusoglu, N. L. Abbott, J. J. de Pablo, Nanoparticle self-assembly at the interface of liquid crystal droplets. *Proc. Natl. Acad. Sci. U.S.A.* **112**, 5297–5302 (2015).
13. J. K. Whitmer, X. Wang, F. Mondiot, D. S. Miller, N. L. Abbott, J. J. de Pablo, Nematic-field-driven positioning of particles in liquid crystal droplets. *Phys. Rev. Lett.* **111**, 227801 (2013).

14. J. Dontabhaktuni, M. Ravnik, S. Žumer, Shape-tuning the colloidal assemblies in nematic liquid crystals. *Soft Matter.* **8**, 1657–1663 (2012).
15. F. Mondiot, S. Prathap Chandran, O. Mondain-Monval, J.-C. Loudet, Shape-induced dispersion of colloids in anisotropic fluids. *Phys. Rev. Lett.* **103**, 238303 (2009).
16. C. P. Lapointe, T. G. Mason, I. I. Smalyukh, Shape-controlled colloidal interactions in nematic liquid crystals. *Science* **326**, 1083–1086 (2009).
17. B. Senyuk, Q. Liu, E. Bililign, P. D. Nystrom, I. I. Smalyukh, Geometry-guided colloidal interactions and self-tiling of elastic dipoles formed by truncated pyramid particles in liquid crystals. *Phys. Rev. E* **91**, 040501 (2015).
18. P. A. Giardini, D. A. Fletcher, J. A. Theriot, Compression forces generated by actin comet tails on lipid vesicles. *Proc. Natl. Acad. Sci. U.S.A.* **100**, 6493–6498 (2003)
19. H. Boukellal, O. Campàs, J.-F. Joanny, J. Prost, C. Sykes, Soft *Listeria*: Actin-based propulsion of liquid drops. *Phys. Rev. E* **69**, 061906 (2004).
20. S. V. Lishchuk, C. M. Care, Shape of an isotropic droplet in a nematic liquid crystal: The role of surfactant. *Phys. Rev. E* **70**, 011702 (2004).
21. N. Sulaiman, D. Marenduzzo, J. M. Yeomans, Lattice Boltzmann algorithm to simulate isotropic-nematic emulsions. *Phys. Rev. E* **74**, 041708 (2006).
22. S. V. Lishchuk, C. M. Care, I. Halliday, A lattice Boltzmann scheme for a nematic–isotropic interface. *J. Phys. Condens. Matter.* **16**, S1931 (2004).
23. N. M. Silvestre, P. Patrício, M. M. Telo da Gama, Elliptical soft colloids in smectic-*C* films. *Phys. Rev. E* **74**, 021706 (2006).
24. P. V. Dolganov, H. T. Nguyen, G. Joly, V. K. Dolganov, P. Cluzeau, Shape of nematic droplets in smectic membranes. *Europhys. Lett.* **78**, 66001 (2006).
25. E. G. Virga, *Variational Theories for Liquid Crystals* (Chapman and Hall, London, 1994).
26. S. Chandrasekhar, Surface tension of liquid crystals. *Mol. Cryst. Liq. Cryst.* **2**, 71–80 (1966).
27. P. Prinsen, P. van der Schoot, Shape and director-field transformation of tactoids. *Phys. Rev. E* **68**, 021701 (2003).
28. Y. Wu, W. Yu, C. Zhou, Y. Xu, Shape evolution of a single liquid- crystal droplet immersed in an isotropic matrix under transient and steady flow. *Phys. Rev. E* **75** (Pt. 1), 041706 (2007).
29. J. Jeong, Z. S. Davidson, P. J. Collings, T. C. Lubensky, A. G. Yodh, Chiral symmetry breaking and surface faceting in chromonic liquid crystal droplets with giant elastic anisotropy. *Proc. Natl. Acad. Sci. U.S.A.* **111**, 1742–1747 (2014).
30. F. C. Keber, E. Loiseau, T. Sanchez, S. J. DeCamp, L. Giomi, M. J. Bowick, M. C. Marchetti, Z. Dogic, A. R. Bausch, Topolgy and dynamics of active nematic vesicles. *Science* **345**, 1135–1139 (2014).
31. G. Wulff, Zur frage der geschwindigkeit des wachstums und der auflösung der krystallflächen. *Zeitschrift für Kristallographie-Crystalline Materials* (New York, Oxford Univ. Press, 1901) pp. 449–530.
32. M. Abkarian, C. Lartigue, A. Viallat, Tank treading and unbinding of deformable vesicles in shear flow: Determination of the lift force. *Phys. Rev. Lett.* **88**, 068103 (2002).
33. A. D. Rey, Mechanics of soft-solid–liquid-crystal interfaces. *Phys. Rev. E* **72** (Pt. 1), 011706 (2005).
34. F. E. Mackay, C. Denniston, Deformable vesicles interacting in a nematic liquid crystal. *Soft Matter.* **9**, 5285–5295 (2013).
35. P. de Gennes, J. Prost, *The Physics of Liquid Crystals* (Oxford Univ. Press, Oxford, 1995), 614 pp.
36. P. Pranay, S. G. Anekal, J. P. Hernández-Ortiz, M. D. Graham, Pair collisions of fluid-filled elastic capsules in shear flow: Effects of membrane properties and polymer additives. *Phys. Fluids* **22**, 123103 (2010).
37. G. A. Buxton, R. Verberg, D. Jasnow, A. C. Balazs, Newtonian fluid meets an elastic solid: Coupling lattice Boltzmann and lattice-spring models. *Phys. Rev. E* **71** (Pt. 2), 056707 (2005).
38. M. M. Dupin, I. Halliday, C. M. Care, L. Alboul, L. L. Munn, Modeling the flow of dense suspensions of deformable particles in three dimensions. *Phys. Rev. E* **75**, 066707 (2007).
39. M. Ravnik, S. Žumer, Landau–de Gennes modelling of nematic liquid crystal colloids. *Liq. Cryst.* **36**, 1201–1214 (2009).
40. M. Papoular, A. Rapini, Surface waves in nematic liquid crystals. *Solid State Commun.* **7**, 1639–1641 (1969).
41. J.-B. Fournier, P. Galatola, Modeling planar degenerate wetting and anchoring in nematic liquid crystals. *Europhys. Lett.* **72**, 403 (2005).
42. C. J. Smith, C. Denniston, Elastic response of a nematic liquid crystal to an immersed nanowire. *J. Appl. Phys.* **101**, 014305 (2007).
43. T. C. Lubensky, D. Pettey, N. Currier, H. Stark, Topological defects and interactions in nematic emulsions. *Phys. Rev. E* **57**, 610–625 (1998).
44. A. D. Rey, Generalized nematostatics. *Liq. Cryst.* **28**, 549–556 (2001).

Acknowledgments: We are grateful to J. C. Armas-Perez for helpful discussions. We thank the NSF for financial support of this work. **Funding:** The fundamental studies of LCs far from equilibrium and the theoretical expressions that relate elastic stress in a LC to torque in suspended particles were supported by NSF DMR-1410674. The theoretical formalism developed here for coupling of membrane shape to liquid crystal stress was supported by DMR-1420709. The calculations and experiments on vesicle deformation by a nematic medium were supported by DMR-1121288. **Author contributions:** R.Z., N.L.A., and J.J.d.P. designed the research; R.Z., J.P.H.-O., and J.J.d.P. developed the model and performed the calculations; N.L.A. performed the experiments; R.Z., Y.Z., J.A.M.-G., J.P.H.-O., N.L.A., and J.J.d.P. contributed to the analysis of the data and discussion of the results; and R.Z., N.L.A., and J.J.d.P. wrote the paper. **Competing interests:** The authors declare that they have no competing interests. **Data and materials availability:** All data needed to evaluate the conclusions in the paper are present in the paper and/or the Supplementary Materials. Additional data related to this paper may be requested from the authors.

Submitted 3 May 2016
Accepted 14 July 2016
Published 10 August 2016
10.1126/sciadv.1600978

Citation: R. Zhang, Y. Zhou, J. A. Martínez-González, J. P. Hernández-Ortiz, N. L. Abbott, J. J. de Pablo, Controlled deformation of vesicles by flexible structured media. *Sci. Adv.* **2**, e1600978 (2016).